



Contents lists available at ScienceDirect

Catalysis Today

journal homepage: [www.elsevier.com/locate/cattod](http://www.elsevier.com/locate/cattod)

# Keggin heteropolyacids supported on TiO<sub>2</sub> used in gas-solid (photo)catalytic propene hydration and in liquid-solid photocatalytic glycerol dehydration

Giuseppe Marci<sup>a,\*</sup>, Elisa García-López<sup>a</sup>, Vincenzo Vaiano<sup>b</sup>, Giuseppe Sarno<sup>b</sup>,  
Diana Sannino<sup>b</sup>, Leonardo Palmisano<sup>a</sup><sup>a</sup> "Schiavello-Grillone" Photocatalysis Group, Dipartimento di Energia, Ingegneria dell'informazione e modelli Matematici (DEIM), Università di Palermo, Viale delle Scienze, 90128 Palermo, Italy<sup>b</sup> Department of Industrial Engineering, University of Salerno, Via Giovanni Paolo II, 84084 Fisciano, Salerno, Italy

## ARTICLE INFO

### Article history:

Received 9 February 2016

Received in revised form 10 April 2016

Accepted 30 April 2016

Available online xxx

### Keywords:

Heteropolyacid

Propene

Glycerol

Photocatalysis

Polyoxometalate

## ABSTRACT

(Photo)catalytic propene hydration to 2-propanol and glycerol dehydration to acrolein were carried out by using Keggin heteropolyacids (HPAs) supported on TiO<sub>2</sub>. Binary materials have been prepared by impregnation of H<sub>3</sub>PW<sub>12</sub>O<sub>40</sub>, H<sub>3</sub>PMo<sub>12</sub>O<sub>40</sub> and H<sub>4</sub>SiW<sub>12</sub>O<sub>40</sub>, on TiO<sub>2</sub> Evonik P25. Moreover, a binary material consisting of H<sub>4</sub>SiW<sub>12</sub>O<sub>40</sub> and TiO<sub>2</sub> was prepared via a hydrothermal treatment and tested for the same reactions. All the materials were characterized by X-ray diffraction (XRD), scanning electron microscopy observations (SEM) coupled with energy dispersive X-ray (EDX) measurements, diffuse reflectance spectroscopy (DRS), Raman spectroscopy and Fourier transform infrared spectroscopy (FTIR). The supported Keggin HPA species played a key role both for the catalytic and for the photo-assisted catalytic reactions due to their strong acidity and ability to form strong oxidant species under UV irradiation.

© 2016 Elsevier B.V. All rights reserved.

## 1. Introduction

Polyoxometalates (POMs) are a wide class of discrete nano-sized transition metal-oxygen clusters that can be divided in three classes: heteropolyanions (HPA), isopolyanions (IPA) and Mo-blue and Mo-brown reduced HPA centers [1]. The most explored POM materials are the HPAs and it is convenient to classify them starting from the symmetrical 'parent' polyanion, for instance the Keggin or Wells-Dawson structures among others [2]. The Keggin anion {XM<sub>12</sub>O<sub>40</sub>}<sup>y-</sup> contains a heteroatom X in the XO<sub>4</sub><sup>y-</sup> centre as PO<sub>4</sub><sup>3-</sup> or SiO<sub>4</sub><sup>3-</sup> and the so-called addenda atoms, commonly W or Mo. For instance, the structure of the PW<sub>12</sub>O<sub>40</sub><sup>3-</sup> anion consists of a PO<sub>4</sub> tetrahedron surrounded by four W<sub>3</sub>O<sub>9</sub> groups formed by edge sharing octahedra. This cluster has a diameter of ca. 1.2 nm [3]. The heteropolyacids with the Keggin structure are strongly acidic and are remarkably stable particularly when deposited onto an oxide surface. They are widely used in catalysis and homogeneous photocatalysis because are very soluble in polar solvents. Heteropolyacids have been used as homogeneous photocatalysts

because their ground electronic state (the solubilized HPA) absorbs light producing a charge transfer-excited state HPA\*. HPA materials, when excited by light to HPA\*, act as better oxidant and reductant species with respect to the corresponding ground states [4]. Indeed, HPA\* can easily become HPA<sup>-</sup>, a "heteropolyblue" specie by means of one (or more) electron transfer from other species [5]. Heteropolyblue species HPA<sup>-</sup> are relatively stable and are readily re-oxidized. Enhanced degradation of organic compounds in the UV/TiO<sub>2</sub> process has been reported in the presence of supported Keggin-type HPAs [6]. In a previous paper the catalytic and catalytic photo-assisted activity of H<sub>3</sub>PW<sub>12</sub>O<sub>40</sub> supported on TiO<sub>2</sub>, ZrO<sub>2</sub> or WO<sub>3</sub> was studied and a beneficial role of the photo-catalytically active support on the reaction rate was reported [7]. The significant increase of reactivity was justified by considering the ability of the semiconductor to transfer electrons from the conduction band to the activated HPA\* species. TiO<sub>2</sub>, in fact, directly transfers photo-generated electrons from its conduction band to the interfacial HPA with empty d orbitals and consequently the electron-hole charge-pairs recombination is delayed [8]. Moreover, the dispersion of HPAs on solid supports with high surface area, is generally useful for improving the accessibility to their acid sites and the (photo)catalytic activity increases.

\* Corresponding author.

E-mail address: [giuseppe.marci@unipa.it](mailto:giuseppe.marci@unipa.it) (G. Marci).

In this paper catalytic photo-assisted activities of  $\text{H}_3\text{PW}_{12}\text{O}_{40}$ ,  $\text{H}_3\text{PMo}_{12}\text{O}_{40}$  and  $\text{H}_4\text{SiW}_{12}\text{O}_{40}$  supported on  $\text{TiO}_2$  have been investigated for two kinds of reactions: i.e. the propene hydration and the glycerol dehydration in gas-solid and in liquid solid regimes, respectively. These reactions are of great interest from the industrial point of view, particularly when carried out under experimental mild conditions. The industrial propene hydration to 2-propanol is carried out at moderate temperatures (ca. 150–200 °C) and under pressure (2 MPa) in the presence of phosphoric acid supported on silica, strong acid resins or zeolites but also heteropolyacids are industrially used for this reaction [9]. Conversely, the dehydration of 2-propanol to form propene is accepted to be a good reaction to probe the acid character of a catalyst [10]. In a gas-solid regime propene and/or propanone are formed at ambient pressure and moderate temperature (in the range 140–325 °C). The selectivity to propene or propanone strongly depends on the acidity-basicity of the solid catalyst. The propene hydration is not an easy reaction to be carried out, because thermodynamically limited by the reverse reaction at high temperature. Intensive research efforts have been also devoted to find new outlets for the high amount of glycerol produced from the biodiesel process [11]. The finding of novel conversion processes to transform glycerol into other chemicals includes scientific efforts in the glycerol dehydration to form acrolein. 3-hydroxypropionaldehyde is obtained after the direct glycerol loss of one water molecule. A further loss of a water molecule gives rise to acrolein. Acrolein is an important chemical used as a feedstock to produce acrylic acid, pharmaceuticals or to treat fibers, and it is also an herbicide which controls the growth of aquatic plants. It is currently produced by oxidation of propene by heterogeneous catalysis. A maximum yield of 80% at high propene conversion (90–95%) is reached by using commercial catalysts based on Bismuth molybdates [12]. Synthesis of acrolein from glycerol has been widely investigated since the 1960's but it has been mainly reported in patent literature. A strong catalyst acidity seems to be necessary to perform the dehydration of glycerol to acrolein in gas phase in the presence of zeolite [13] or in supercritical water [14] by using various solid acid catalysts including sulphates. Chai et al. reported the gas-phase dehydration of glycerol to produce acrolein at 315 °C by using  $\text{Nb}_2\text{O}_5$  [15,16]. Glycerol conversion and acrolein selectivity of the  $\text{Nb}_2\text{O}_5$  catalysts were dependent on the fraction of strong acid sites ( $-8.2 \leq H_0 \leq -3.0$ ), where  $H_0$  corresponds to the Hammett factor. The amorphous catalyst prepared by calcination at 400 °C, having the highest fraction of acid sites at  $-8.2 \leq H_0 \leq -3.0$ , showed the highest mass specific activity and acrolein selectivity (51 mol%). The other samples, having a higher fraction of either stronger ( $H_0 \leq -8.2$ ) or weaker acid sites ( $-3.0 \leq H_0 \leq 6.8$ ), were less effective for glycerol dehydration and formation of the desired acrolein. The highest selectivity was ca. 70 mol%. The catalysts having further stronger acid sites ( $H_0 \leq -8.2$ ) produce a lower selectivity (40–50 mol%) due to a more severe catalyst coking. Authors evidenced that Brønsted acid sites presented better performance than Lewis acid sites. Chai et al. proposed a mechanism where the reaction was initiated by the dehydration involving either the central or a terminal –OH of glycerol which result in the parallel formation of two enol intermediates. The enols would undergo rapid rearrangement to 3-hydroxypropionaldehyde or 1-hydroxyacetone, respectively. The 3-hydroxypropionaldehyde would be very unstable at the reaction temperature (315 °C) and it can easily give rise to a further dehydration to acrolein. A secondary hydrogenation reaction of the acrolein product will lead to the formation of allyl alcohol. The unstable intermediate 3-hydroxypropionaldehyde would also decompose to acetaldehyde and formaldehyde, according to a reversed aldol condensation; a follow up hydrogenation or decomposition of formaldehyde would result in the formation of methanol or CO and  $\text{H}_2$ .

Tsukuda et al. investigated the production of acrolein from glycerol over silica-supported heteropoly acids [17]. In that study, silicotungstic acid supported on silica with mesopores of 10 nm showed the highest catalytic activity with the acrolein selectivity <85 mol% at 275 °C and at ambient pressure.

Shen et al. studied the catalytic activities of silicotungstic, phosphotungstic, and phosphomolybdic acids in the liquid phase dehydration of glycerol to acrolein in a semi-batch reactor [18]. Silicotungstic acid exhibited high catalytic activity and the maximum yield of 78.6% was achieved when glycerol was completely converted at the reaction temperature of 300 °C with the mole ratio of silicotungstic acid to glycerol of  $1 \cdot 10^{-4}:1$ . The order of catalytic activities toward the formation of acrolein was silicotungstic acid > phosphotungstic acid > phosphomolybdic acid, revealing that the reaction was affected by the acidity and the stability of the heteropolyacids. Hydroxyacetone and acetic acid were also detected with yields of less than 10%, respectively.

Liu et al. studied  $\text{Al}_2\text{O}_3$  supported silicotungstic acid ( $\text{H}_4\text{SiW}_{12}\text{O}_{40}/\text{Al}_2\text{O}_3$ ) samples prepared by impregnation and calcined at 350, 450, 550, 650 °C to study the structural evolution of the  $\text{H}_4\text{SiW}_{12}\text{O}_{40}$  heteropolyacid and its effect on the catalytic performance during glycerol conversion to acrolein in gas-solid regime at 300 °C [19]. The glycerol conversion increased with acid center concentration under the specified reaction condition. As well, selectivity to acrolein increased with Brønsted/Lewis acid ratio, suggesting the crucial role of Brønsted acid sites.

In this paper some bulk and surface properties of three heteropolyacid clusters supported on  $\text{TiO}_2$  materials have been studied along with their use as heterogeneous photocatalysts in two reactions, i.e. the propene hydration and the glycerol dehydration. The investigation focuses how the (photo)reactivity can depend on the type of HPA but also how the support-heteropolyacid interaction can be important. As far as the glycerol dehydration is concerned, it is worth nothing that, contrarily to what reported in studies on thermal catalysis, in our UV irradiated system the reaction proceeded at very low temperature (35 °C).

## 2. Experimental

### 2.1. Preparation of the binary HPA/ $\text{TiO}_2$ samples

The binary materials HPA/ $\text{TiO}_2$  were prepared by impregnating the support (commercial  $\text{TiO}_2$  Evonik P25) with an aqueous solution containing the desired amount of the commercial HPA, i.e.  $\text{H}_3\text{PW}_{12}\text{O}_{40}$ ,  $\text{H}_3\text{PMo}_{12}\text{O}_{40}$  or  $\text{H}_4\text{SiW}_{12}\text{O}_{40}$  (Aldrich) denoted hereafter as  $\text{PW}_{12}$ ,  $\text{PMo}_{12}$  and  $\text{SiW}_{12}$ , respectively. During the preparation, each suspension was stirred at 50 °C for 1 h, and then water was evaporated until dryness. The binary materials prepared as above described are denoted hereafter as  $\text{PW}_{12}/\text{TiO}_2$ ,  $\text{PMo}_{12}/\text{TiO}_2$  and  $\text{SiW}_{12}/\text{TiO}_2$ . The HPA amount deposited was 50% in weight with respect to the support corresponding to a molar percentage of 14% of W and 86% of Ti (with respect to the sum W + Ti) in  $\text{PW}_{12}/\text{TiO}_2$  and  $\text{SiW}_{12}/\text{TiO}_2$  samples and 20% of Mo and 80% of Ti (with respect to the sum Mo + Ti) in  $\text{PMo}_{12}/\text{TiO}_2$  sample.

The theoretical coverage of the support has been calculated by taking into account that the diameter of each anionic HPA cluster is equal to ca. 10 Å and, consequently, by considering a roundish shape of the heteropolyanion, its surface area results ca. 78.5 Å<sup>2</sup> [3].

An alternative binary material has been prepared starting from a selected HPA ( $\text{SiW}_{12}$ ) and a  $\text{TiO}_2$  precursor, by using the following methodology. A solution was prepared by adding 7.5 ml of titanium isopropoxide (TTIP) to 50 ml of 2-propanol, hence 6 ml of  $\text{HNO}_3$  0.05 M and the appropriate amount of  $\text{SiW}_{12}$  (0.5440 g) were added under vigorous stirring to the Ti containing solu-

tion. A gel was formed and it was successively introduced in an autoclave internally covered by Teflon. The tightly closed system was heated for 48 h at 200 °C, achieving a final pressure of ca. 10 bar. The solid collected from the autoclave was washed four times with hot water, dried and annealed at 110 °C for 12 h. The molar ratios of the reagents TTIP:2-propanol:HNO<sub>3</sub>:H<sub>2</sub>O:HPA were 155:4000:18:2000:1, corresponding to a molar percentage of 8% of W and 92% of Ti (with respect to the sum W+Ti). This material is denoted as SiW<sub>12</sub>/TiO<sub>2</sub>-H where H means hydrothermal. The reason to prepare a selected HPA supported material under hydrothermal conditions was justified because leaching of HPA (from sample obtained by simple impregnation) has been often observed, due to the high solubility of HPA in polar reaction media. A markedly increased stability of the hydrothermally prepared binary materials HPA-TiO<sub>2</sub>, instead, has been reported by Guo and Hu [20], Ma et al. [21] and Sivakumar et al. [22]. For the sake of comparison a TiO<sub>2</sub> bare sample (named TiO<sub>2</sub>-H) was also prepared by means of the above hydrothermal method.

## 2.2. Characterization of the photocatalysts

Determination of BET specific surface area (SSA) was performed by using a Flowsorb 2300 (Micromeritics). The crystalline phase of the prepared materials was determined at room temperature by powder X-ray diffraction analysis (PXRD) carried out by using a Panalytical Empyrean, equipped with CuK $\alpha$  radiation and PixCel1D (tm) detector. Scanning electron microscopy observations (SEM) were carried out by using a FEI Quanta 200F ESEM microscope, operating at 30 kV on specimens coated with a layer of gold. Moreover, an electron microprobe used in an energy dispersive mode (EDX) was employed to obtain information on the atomic content of W or Mo and Ti on the samples. Raman spectra were recorded on pure powdered samples packed into sample cups. Spectra were recorded by a Reinshaw in-via Raman spectrometer equipped with an integrated microscope and with a charged-coupled device (CCD) camera. A He/Ne laser operating at 632.8 nm was used as the exciting source. Diffuse reflectance spectra (DRS) were recorded in the range 250–600 nm by using a Shimadzu UV-2401 PC instrument with BaSO<sub>4</sub> as the reference sample. Infrared spectra of the samples in KBr (Aldrich) pellets were obtained by using a FTIR-8400 Shimadzu spectrometer with 4 cm<sup>-1</sup> resolution and 256 scans.

The acidity of the samples were studied by the dehydration reaction of 2-propanol to propene. To this scope it was used a cylindrical Pyrex batch reactor (V = 130 ml, external diameter = 93 mm, external height = 22 mm) provided with a silicon/teflon septum. The photocatalyst (0.1 g) was placed on the bottom of the photoreactor and N<sub>2</sub> was fluxed for ca. 0.5 h to remove the oxygen. Subsequently, 10  $\mu$ l of liquid 2-propanol was injected and vaporized into the reactor (2-propanol nominal initial concentration equal to 1.0  $\times$  10<sup>-3</sup> M). After that, the reactor was heated at 80 °C in an oven and the reacting fluid was analysed by withdrawing gas samples from the photoreactor by means of a gas-tight syringe (the runs lasted ca. 4 h). Substrate and propene concentrations were measured by using a GC-17A Shimadzu gas chromatograph equipped with a methyl siloxane (30 m  $\times$  320  $\mu$ m  $\times$  0.25  $\mu$ m) HP-1 column kept at 40 °C and a FID. The acidity of the samples was correlated with the amount of propene formed (higher amount indicating higher acidity).

## 2.3. Reactivity experiments

### 2.3.1. Photocatalytic propene hydration in gas-solid regime

A cylindrical continuous Pyrex photoreactor horizontally positioned (diameter: 10 mm, length: 100 mm) was used and it operated in gas-solid regime. The reactivity runs were carried out with 0.5 g of powder by simply dispersing it as a thin layer inside the

photoreactor (the fixed bed height was ca. 0.3 mm). The gas feeding the photoreactor consisted of propene and water with molar concentrations of ca. 40 mM and ca. 2 mM, respectively. A mass flow controller allowed to feed gaseous propene, whereas water was mixed with the propene stream by means of a home made infusion pump. A porous glass septum allowed to distribute homogeneously the inlet gaseous mixture. The flow rate of the gaseous stream for the catalytic and catalytic photo-assisted runs was 20 cm<sup>3</sup> min<sup>-1</sup>. All of the runs were carried out at atmospheric pressure. The reactor and the pipes of the set-up to and from the reactor were heated by an electric resistance and K-type thermocouples allowed to monitor the temperature in the whole system. The temperature inside the (photo)-reactor was maintained constant at 85 °C for both catalytic and photocatalytic experiments. For the catalytic photo-assisted runs the reactor was illuminated from the top with an UV LED IRIS 40 with an irradiation peak centered at 365 nm. The irradiance reaching the photoreactor, measured in the range 300–400 nm with a UVX Digital radiometer, was equal to 45 mW cm<sup>-2</sup>. The runs lasted ca. 5 h and samples of the reacting fluid were analysed by the same gas chromatograph above described.

### 2.3.2. Photocatalytic glycerol dehydration in liquid-solid regime

The photocatalytic dehydration of glycerol to acrolein was carried out in liquid phase. The experiments were performed by using a Pyrex cylindrical photoreactor (ID = 2.5 cm) equipped with a He distributor device (Q<sub>He</sub> = 200 cm<sup>3</sup> min<sup>-1</sup>, STP) that provided a continuous flow inside the reactor throughout the runs. A magnetic stirrer maintained 0.1 g of photocatalyst suspended in 100 ml aqueous solution containing 0.4 mol of glycerol (Sigma-Aldrich). The dosage equal to 1 g L<sup>-1</sup> ensured that the overall photocatalysts particles were effectively irradiated [23]. The suspension was left under dark for 1 h to reach the adsorption-desorption equilibrium of glycerol on the photocatalyst surface. Then the photoreactor was externally irradiated for 65 min by four Philips Black Light UV tubes (8 W each; emission spectrum centered at 365 nm) and the flux impinging the external surface of the photoreactor was equal to ca. 51 mW cm<sup>-2</sup>. The temperature inside the photo-reactor reached the value of 35 °C. The volatile reaction species formed during the photoreaction in the liquid-solid system were stripped by a He stream bubbled in the suspension. The composition of the reaction products in the liquid phase was analysed by gas chromatography (GC) with a Thermo TR-WaxMS column coupled to a quadrupole mass detector (Trace MS; ThermoFinnigan). Moreover, the gaseous products (CO<sub>2</sub> and CO) in the He stream from the photoreactor were also analysed. The temperature ramp for the GC-MS analyses was 50–250 °C (10 °C min<sup>-1</sup>) followed by 1 min at isothermal conditions.

The percentage of glycerol conversion (X) and of acrolein yield (Y) were used as the parameters to evaluate the photocatalysts performance. They were calculated according to the following equations:

$$X = \frac{n_{GL,in} - n_{GL,un}}{n_{GL,in}} \times 100 \quad (1)$$

$$Y = \frac{n_{AC}}{n_{GL,in}} \times 100 \quad (2)$$

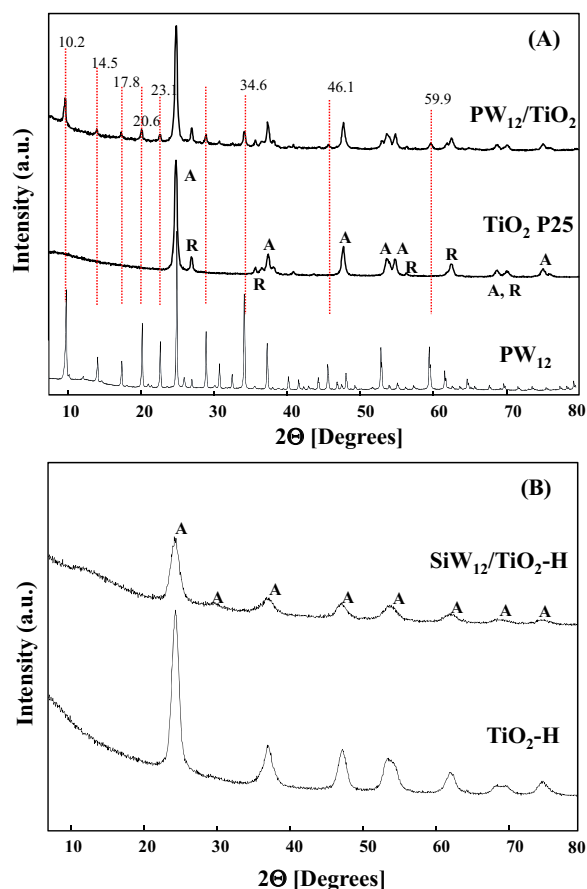
The percentage of selectivity (S) to acrolein was also calculated as follows:

$$S = \frac{n_{AC}}{(n_{GL,in} - n_{GL,un})} \times 100 \quad (3)$$

where  $n_{GL,in}$  is the glycerol initial moles,  $n_{GL,un}$  the moles of glycerol unreacted and still present in the reaction medium after the run and  $n_{AC}$  the moles of produced acrolein.

**Table 1**  
BET specific surface areas (SSA) and band gap energies ( $E_{\text{gap}}$ ) of the photocatalysts.

Sample	B.E.T. SSA [ $\text{m}^2 \text{g}^{-1}$ ]	$E_{\text{gap}}$ [eV]
TiO <sub>2</sub> -Evonik P25	50	3.1 and 3.25
PW <sub>12</sub> /TiO <sub>2</sub>	48	3.0
PMo <sub>12</sub> /TiO <sub>2</sub>	46	2.5 and 2.9
SiW <sub>12</sub> /TiO <sub>2</sub>	47	3.1
TiO <sub>2</sub> -H	180	3.25
SiW <sub>12</sub> /TiO <sub>2</sub> -H	177	3.2

**Fig. 1.** XRD patterns of the photocatalysts: PW<sub>12</sub>, TiO<sub>2</sub> P25, and PW<sub>12</sub>/TiO<sub>2</sub> (A); TiO<sub>2</sub>-H and SiW<sub>12</sub>/TiO<sub>2</sub>-H (B).

### 3. Results and discussion

#### 3.1. Physico-chemical characterization of the materials

Table 1 shows the BET specific surface area (SSA) of all the binary materials along with the commercial support (SSA of all of the HPAs used was ca. 10 m<sup>2</sup> g<sup>-1</sup>). The binary materials prepared under hydrothermal conditions showed higher SSA's. As a general trend, the surface areas of all of the materials are smaller than those of the support.

In Fig. 1(A) the XRD diffractograms of PW<sub>12</sub>, TiO<sub>2</sub> P25 and PW<sub>12</sub>/TiO<sub>2</sub> samples are reported. The heteropolyacid cluster presents a crystalline structure characterized by several diffraction peaks. In the diffractogram of the commercial TiO<sub>2</sub> P25, anatase (A) and rutile (R) polymorphs can be identified. In the composite material diffraction peaks attributable to TiO<sub>2</sub> are present along with some others corresponding to the heteropolyacid cluster (vertical lines).

The XRD patterns of the other impregnated samples, not reported for the sake of brevity, showed also the presence of diffrac-

tion peaks attributable to TiO<sub>2</sub> and to the heteropolyacid. Fig. 1(B) shows the diffractograms of the hydrothermally home prepared bare TiO<sub>2</sub> (TiO<sub>2</sub>-H) and of the composite SiW<sub>12</sub>/TiO<sub>2</sub>-H. In both the diffractograms the presence of anatase phase can be noticed without significant differences and any other peaks ascribable to the heteropolyacid. This finding, confirmed by SEM study, as reported in the following, can be explained considering a good dispersion of the heteropolyacid in the material prepared hydrothermally. However, the possibility that a fraction of HPA was included in the core of the TiO<sub>2</sub> material during the solvothermal preparation of the composite, cannot be excluded.

SEM microphotographs of some selected HPA/TiO<sub>2</sub> materials are reported in Fig. 2(a–d). The morphology of the HPA/TiO<sub>2</sub> samples obtained by HPA impregnation is very similar to that of the bare TiO<sub>2</sub> P25 used as support (SEM picture of bare TiO<sub>2</sub> P25 has been already reported in a previous paper [24]), since the agglomerates of these particles present the same shape and consist of nanoparticles with similar sizes (ca. 50 nm).

Fig. 2(a) and (b) report pictures of PMo<sub>12</sub>/TiO<sub>2</sub>, selected as representative of the impregnated samples, with two different magnifications. As far as the SiW<sub>12</sub>/TiO<sub>2</sub>-H sample is concerned, SEM analysis evidenced the nanostructured nature of the material; indeed it consisted of big agglomerates of particles the dimension of which ranges between 20 and 60 nm. Moreover, interstitial spaces (6–10 nm) can be noticed between the particles.

Table 2 reports the nominal and the average EDX values of atomic percentage of W or Mo from HPA and the atomic percentage of Ti from the support, calculated by taking into account the presence of thirteen water moles per mole of HPA [25]. The amounts of tungsten or molybdenum from HPA measured by EDX analyses resulted close to the nominal ones. Moreover a quite homogeneous distribution of HPA on the TiO<sub>2</sub> was evidenced.

Fig. 3 shows the Raman spectra of bare HPA and supported samples. The former shows the characteristic bands corresponding to anatase and rutile crystalline phases of the TiO<sub>2</sub>. Raman bands at 395, 516 and 637 cm<sup>-1</sup> are clearly present in all the supported materials and assigned to modes of TiO<sub>2</sub> anatase [26]. The rutile phase shows peaks at 444 cm<sup>-1</sup> and at 609 cm<sup>-1</sup>; however in Fig. 3, the first one is present as a shoulder and the second is masked by the anatase peak at 637 cm<sup>-1</sup>. Intense peaks at 142 and 144 cm<sup>-1</sup>, assigned to rutile and anatase, respectively, are out of the range of the spectra reported in Fig. 3. For the three HPA supported samples the characteristic bands attributable to the vibrational modes of the heteropolyacid cluster are also present. The bare PW<sub>12</sub> Raman spectrum is reported in Fig. 3(A). It exhibits a strong W–O symmetric and asymmetric stretching modes at 1012 and 990 cm<sup>-1</sup>, respectively. The bands centered at 937 and 890 cm<sup>-1</sup> are attributed to W–O–W asymmetric stretching. The weaker Raman bands centered at 530 cm<sup>-1</sup> are characteristic of asymmetric stretching vibration modes of bridging W–O–W. The group centered at 325 cm<sup>-1</sup> are attributed to W–O bending [27]. After impregnation on the TiO<sub>2</sub>, no significant shift was observed in the PW<sub>12</sub>/TiO<sub>2</sub> sample for the sharper and more intense bands at 1012 and 990 cm<sup>-1</sup>, whereas the Raman peaks corresponding to the W–O–W asymmetric and symmetric stretching vibration modes were broadened and became relatively weaker with respect to the PW<sub>12</sub> spectrum. Consequently the resolution between these peaks decreases. These findings can be attributed to H-bonding interaction between the oxygen atom of the Keggin anion and the hydroxyl groups on the TiO<sub>2</sub> surface, as observed before [28]. The Raman spectrum of bare PMo<sub>12</sub>, reported in Fig. 3(B), showed bands at 995 and 983 cm<sup>-1</sup> that are assigned to symmetric and asymmetric stretching of terminal oxygen Mo–O. The weak band at 882 cm<sup>-1</sup> can be assigned to Mo–O–Mo asymmetric stretching, whereas the band at 603 cm<sup>-1</sup> to a combined stretching and bending of the Mo–O–Mo bonds [29,30]. In Fig. 3(B) the comparison between the

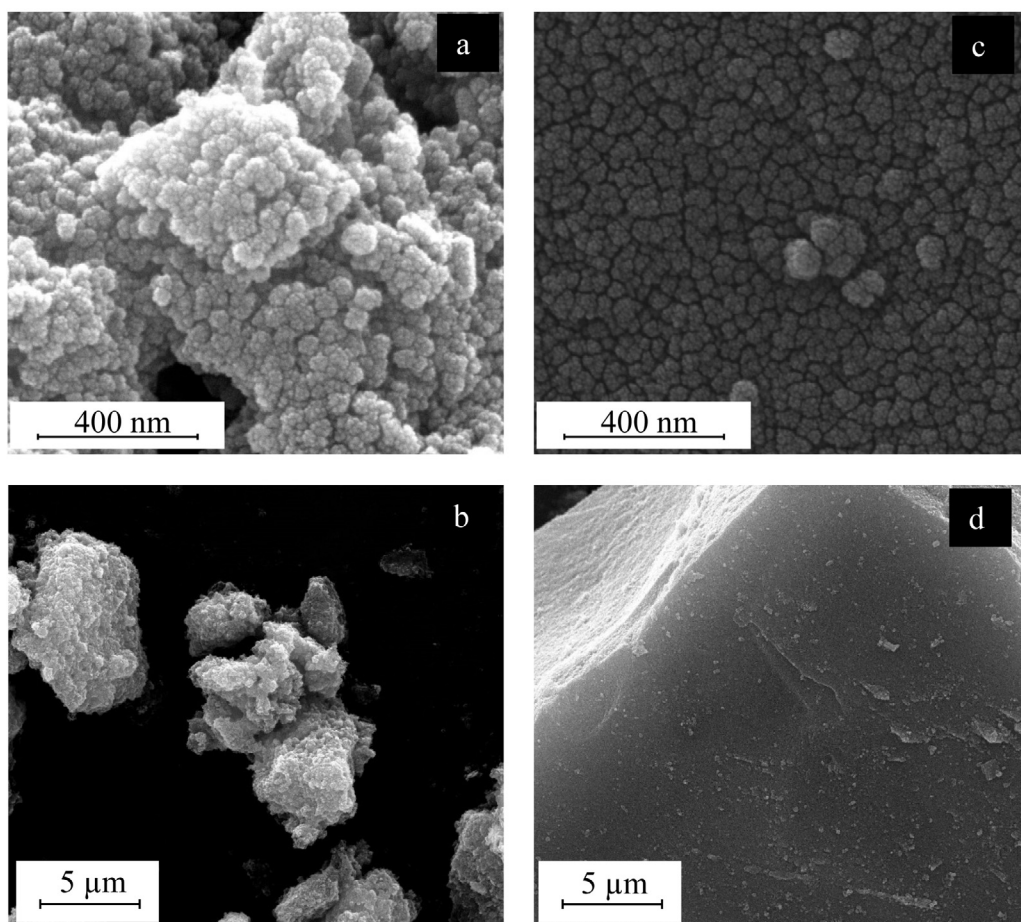


Fig. 2. SEM pictures of two selected samples, each with two different magnifications:  $\text{PMo}_{12}/\text{TiO}_2$  (a) and (b) and  $\text{SiW}_{12}/\text{TiO}_2\text{-H}$  (c) and (d).

Table 2

Atomic percentage of Ti and W or Mo (with respect to the sum Ti + W or Ti + Mo), both nominal and measured by EDX analyses and theoretical HPA coverage on the support.

Sample	Ti atomic percentage		W or Mo atomic percentage		Theoretical coverage HPA layers
	nominal	EDAX	nominal	EDAX	
$\text{PW}_{12}/\text{TiO}_2$	86	83	14	17	2.8
$\text{PMo}_{12}/\text{TiO}_2$	80	83	20	17	4.5
$\text{SiW}_{12}/\text{TiO}_2$	86	83	14	17	2.8
$\text{SiW}_{12}/\text{TiO}_2\text{-H}$	92	92	8	8	n.c. <sup>a</sup>

<sup>a</sup> Not calculated because the preparation was carried out by using a different method with respect to the other samples reported in Table 2 (see Section 2).

Raman spectrum of the bare  $\text{PMo}_{12}$  heteropolyacid cluster with the  $\text{PMo}_{12}$  impregnated on  $\text{TiO}_2$  evidences, analogously to what occurs in the case of the  $\text{PW}_{12}$ , that in the supported material both the bands of  $\text{TiO}_2$  and those related to the heteropolyacid are present without significant shifts with respect to the bare  $\text{PMo}_{12}$ . Only an enlargement of the bands due to an interaction between the cluster and the support is evident. Fig. 3(C) illustrates the differences between the bare  $\text{SiW}_{12}$  cluster and the materials containing  $\text{TiO}_2$ . The Raman vibrational modes typically assigned to the Keggin anion are those located at 1019, 981, 927, 881  $\text{cm}^{-1}$ , attributed to symmetrical and asymmetrical stretching W–O and W–O–W modes [31]. Significant differences are evidenced in Fig. 3(C) among the three samples. In fact, for the  $\text{SiW}_{12}/\text{TiO}_2$  and  $\text{SiW}_{12}/\text{TiO}_2\text{-H}$  materials a clear enlargement of the bands attributable to the vibrational modes of  $\text{SiW}_{12}$  can be observed along with a shift, which increases in the case of  $\text{SiW}_{12}/\text{TiO}_2\text{-H}$ . This indicates a different interaction between the support and  $\text{SiW}_{12}$  in the  $\text{TiO}_2$  containing materials [28,32]. The samples were also investigated by FTIR to check the structural integrity of the Keggin unit after the prepa-

ration of the HPA/ $\text{TiO}_2$  composites. The arrangement structure of the  $\text{PW}_{12}$  consists of a  $\text{PO}_4$  tetrahedron surrounded by four  $\text{W}_3\text{O}_9$  groups formed by edge sharing octahedra [33]. This arrangement gives rise to four stretching bands between 1100 and 700  $\text{cm}^{-1}$ , the fingerprint region for this kind of compounds. The presence of the  $\text{TiO}_2$  cut-off at wavenumbers lower than 900  $\text{cm}^{-1}$  does not allow to clearly notice part of these range. The characteristic bands of Keggin ions have been assigned according to Rocchiccioli-Deltcheff et al. [34].

Fig. 4(A) shows the vibration modes of the bare  $\text{PW}_{12}$  cluster where the P–O stretching mode is observed at 1080  $\text{cm}^{-1}$ , W=O asymmetric stretching at 990 and 982  $\text{cm}^{-1}$  and a peak at ca. 890  $\text{cm}^{-1}$  along with a wide band centred at ca. 800  $\text{cm}^{-1}$  which can be attributed to two types of asymmetric stretching of W–O–W units.

The presence of two bands or a wide one can be explained with the existence of two kinds of tungsten chains, i.e. W–O<sub>c</sub>–W and W–O<sub>b</sub>–W where the O<sub>c</sub> oxygen atom is common for two  $[\text{WO}_6]$  octahedra in  $[\text{W}_3\text{O}_{10}]$  subunits, joined by O<sub>b</sub> atoms. These main

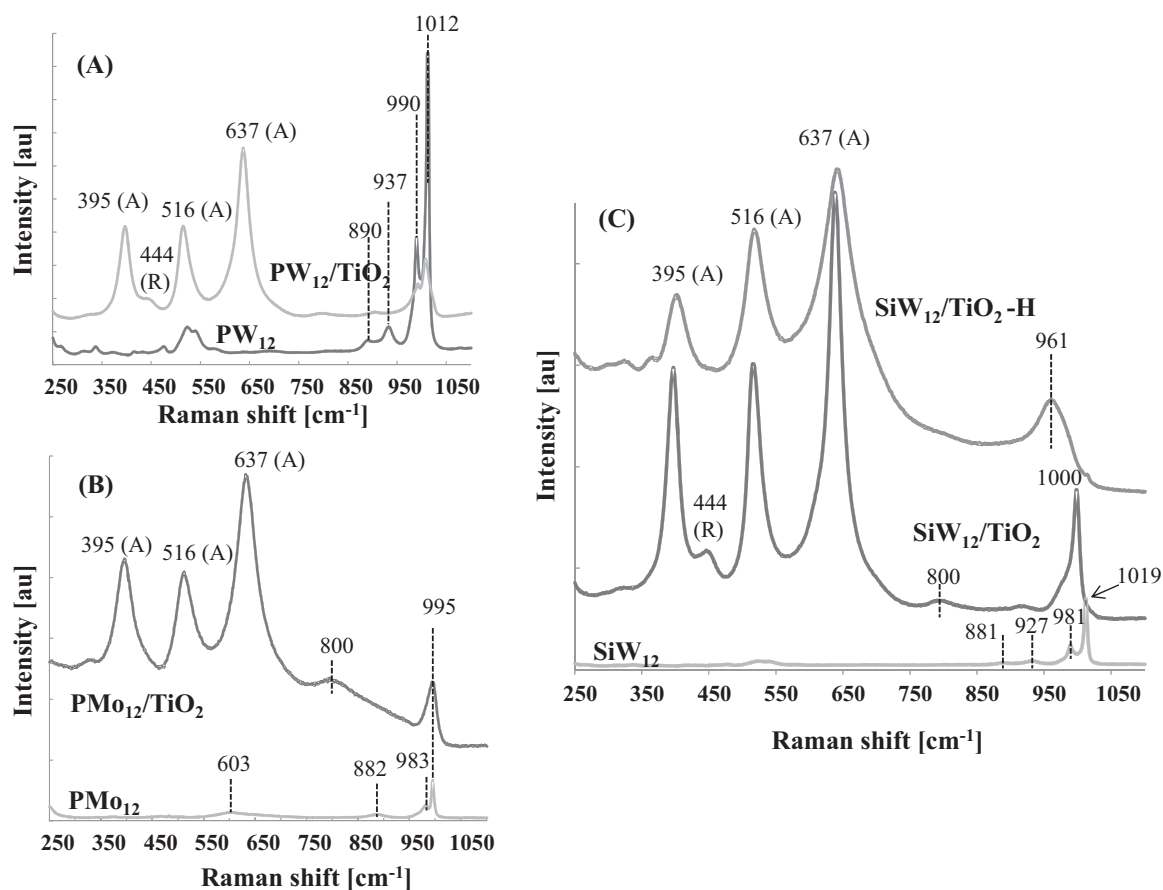


Fig. 3. Raman spectra of: PW<sub>12</sub> and PW<sub>12</sub>/TiO<sub>2</sub> (A); PMo<sub>12</sub> and PMo<sub>12</sub>/TiO<sub>2</sub> (B); SiW<sub>12</sub>, SiW<sub>12</sub>/TiO<sub>2</sub> and SiW<sub>12</sub>/TiO<sub>2</sub>-H (C).

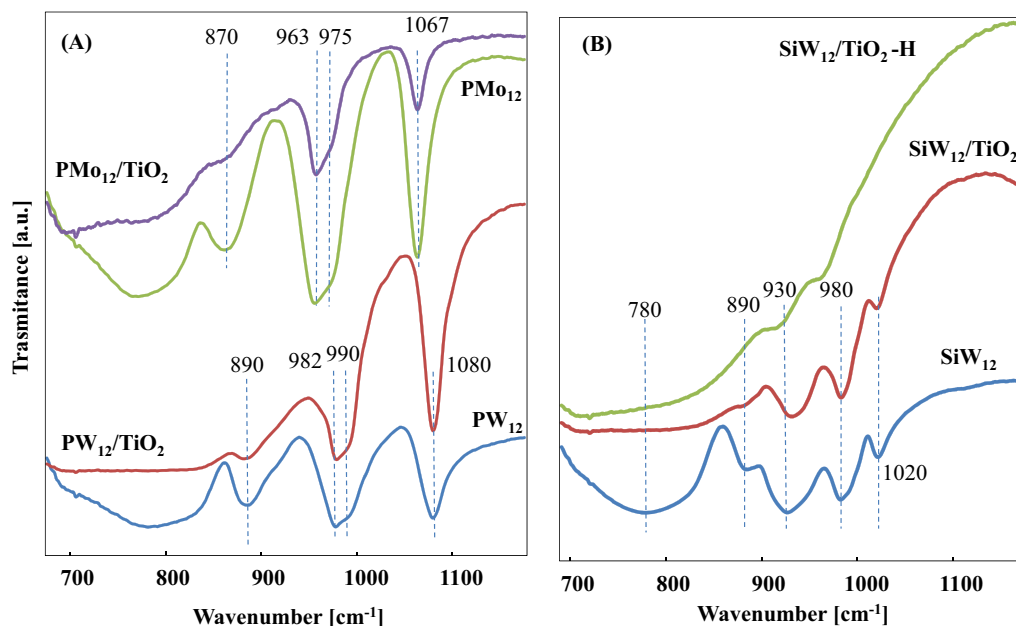


Fig. 4. FTIR spectra of PW<sub>12</sub>, PW<sub>12</sub>/TiO<sub>2</sub>, PMo<sub>12</sub> and PMo<sub>12</sub>/TiO<sub>2</sub> (A); SiW<sub>12</sub>, SiW<sub>12</sub>/TiO<sub>2</sub> and SiW<sub>12</sub>/TiO<sub>2</sub>-H (B).

stretching vibrations of the skeletal bonds in PW<sub>12</sub> are located at the same wavenumbers when the cluster is loaded on the surface of TiO<sub>2</sub>, indicating that the Keggin geometry of PW<sub>12</sub> is preserved in the binary material although the presence of the TiO<sub>2</sub> cut-off intense and broad vibration band, originated from Ti–O–Ti bonds

and located at wavenumbers lower than 900 cm<sup>-1</sup>, does not allow to clearly notice the last wide band attributable to the asymmetric stretching of W–O–W units. As far as the bare PMo<sub>12</sub> cluster is concerned, also in Fig. 4(A) a band attributed to the P–O stretching (1067 cm<sup>-1</sup>) is displayed, along with the Mo=O stretching (975 and

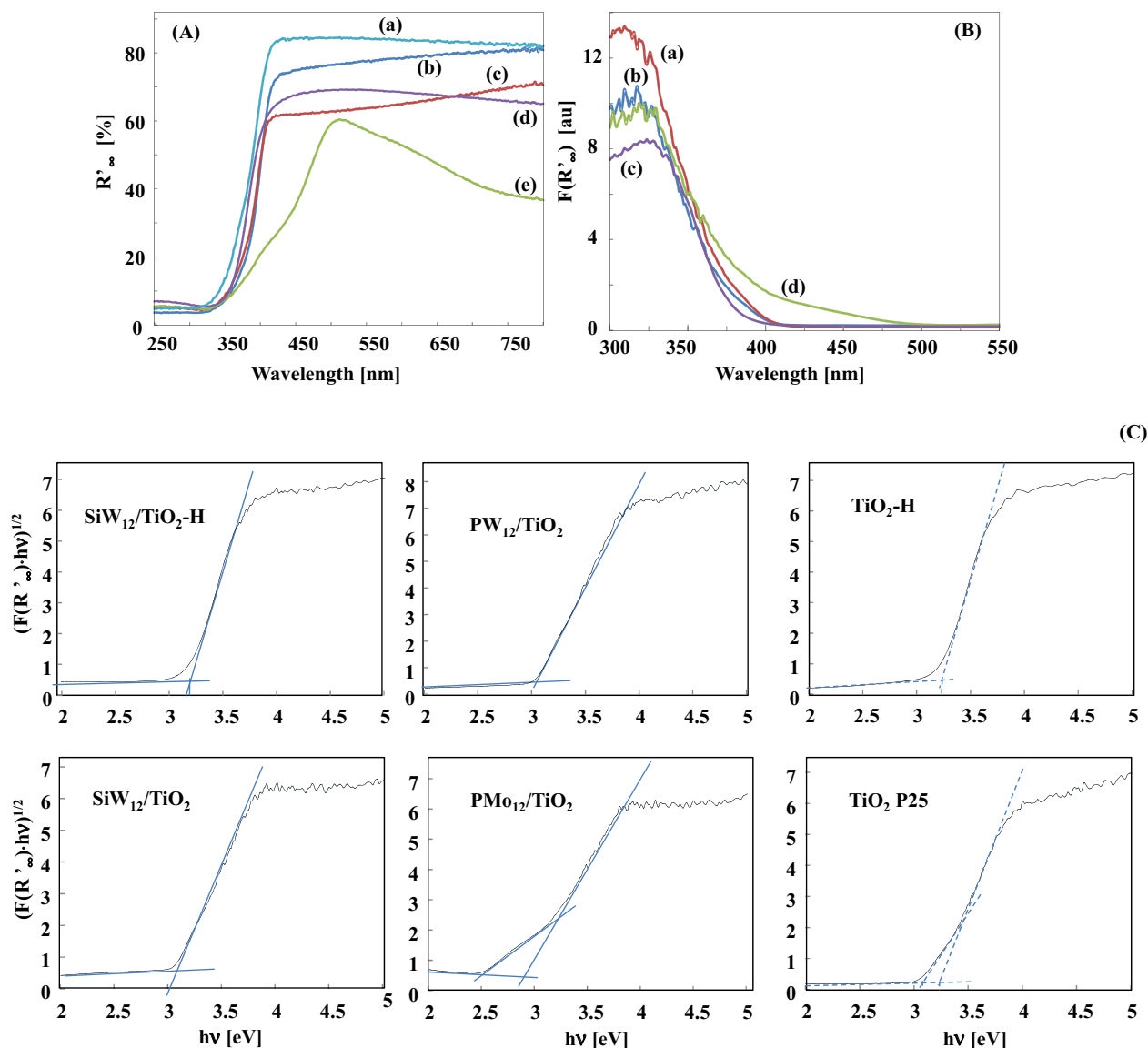


Fig. 5. (A) DRS spectra of TiO<sub>2</sub> P25 (a); PW<sub>12</sub>/TiO<sub>2</sub> (b); SiW<sub>12</sub>/TiO<sub>2</sub> (c); SiW<sub>12</sub>/TiO<sub>2</sub>-H (d) and PMo<sub>12</sub>/TiO<sub>2</sub> (e); (B) absorbance spectra of PW<sub>12</sub>/TiO<sub>2</sub> (a); SiW<sub>12</sub>/TiO<sub>2</sub> (b); SiW<sub>12</sub>/TiO<sub>2</sub>-H (c); PMo<sub>12</sub>/TiO<sub>2</sub> (d); (C) Tauc plots for all of the photocatalysts used.

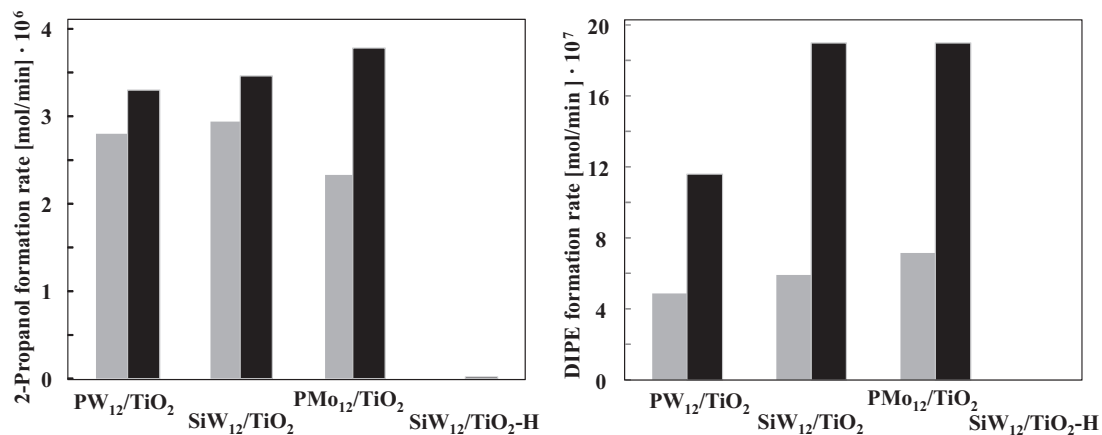


Fig. 6. 2-Propanol and isopropylether (DIPE) formation rates by using the various HPA supported materials for the catalytic (grey bars) and catalytic photo assisted (black bars) propene hydration reaction.

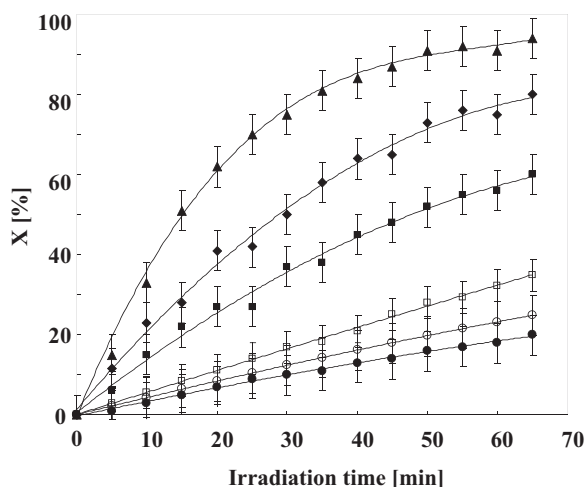


Fig. 7. Glycerol conversion (X%) versus irradiation time for runs carried out in the presence of:  $\text{PMo}_{12}/\text{TiO}_2$  (▲);  $\text{SiW}_{12}/\text{TiO}_2$  (◆);  $\text{PW}_{12}/\text{TiO}_2$  (■);  $\text{TiO}_2$  P25 (□);  $\text{TiO}_2$ -H (○) and in the absence of photocatalyst (●).

$963\text{ cm}^{-1}$ ). The peaks at ca.  $870$  and the wide band centred at ca.  $790\text{ cm}^{-1}$  [34] attributable to two types of  $\text{Mo}-\text{O}-\text{Mo}$  units are also present. Also in this case the main vibration modes of the  $\text{PMo}_{12}$  cluster are not shifted when the heteropolyanion is supported on  $\text{TiO}_2$ .

The FTIR spectra of bare  $\text{SiW}_{12}$ ,  $\text{SiW}_{12}/\text{TiO}_2$  and  $\text{SiW}_{12}/\text{TiO}_2$ -H are shown in Fig. 4(B). The bare  $\text{SiW}_{12}$  spectrum presents five characteristic vibration modes located at  $780$ ,  $890$ ,  $930$ ,  $980$ , and  $1020\text{ cm}^{-1}$ . The bands at  $780$  and  $890\text{ cm}^{-1}$  correspond to stretching of  $\text{W}-\text{O}-\text{W}$  chains, those at  $930\text{ cm}^{-1}$  and  $980\text{ cm}^{-1}$  to  $\text{Si}-\text{O}$  and  $\text{W}=\text{O}$  stretchings, respectively [34,35]. The  $1020\text{ cm}^{-1}$  band has been previously observed, however its assignment is unknown [36] and it could be attributed to an impurity adsorbed on the acidic sites of the HPA. In the spectrum of  $\text{SiW}_{12}/\text{TiO}_2$  sample only the band corresponding to the  $\text{Si}-\text{O}$  stretching presents a shift with respect to the bare  $\text{SiW}_{12}$ . On the contrary, the location of the bands in the  $\text{SiW}_{12}/\text{TiO}_2$ -H accounts for some distortion or modification of the cluster in the sample in agreement with the Raman results.

Fig. 5(A) and (B) report the diffuse reflectance UV-vis spectra (DRS) and the absorption (reported as  $F(R'_{\infty})$ ), respectively, of the bare  $\text{TiO}_2$  and  $\text{HPA}/\text{TiO}_2$  supported samples. The samples are characterized by a charge transfer process from  $\text{O } 2p$  to  $\text{Ti } 3d$  corresponding to the  $\text{TiO}_2$  band gap values (ca.  $3.2\text{ eV}$  for anatase and  $3.0\text{ eV}$  for rutile). The band gap energies of the samples have been estimated (see Table 1) from the tangent lines in the plots of the modified Kubelka–Munk function,  $[F(R'_{\infty})h\nu]^{1/2}$ , versus the energy of exciting light reported in Fig. 5(C) [36]. The presence of the HPA gave rise to a slight decrease of the band gap energy only for  $\text{PMo}_{12}/\text{TiO}_2$  sample that presented a second band gap due to the presence of the HPA. By taking into account all the above physico-chemical characterization results, it can be concluded that the primary Keggin structure of the HPA remained virtually unchanged after the deposition of the cluster on the oxide surface except for the hydrothermally prepared material, but at the same time, based on the spectroscopic results, an interaction between the Keggin unit and the  $\text{TiO}_2$  surface can be hypothesized.

As far as the tests devoted to understand the acidity of the samples are concerned, they indicate that the acidity decreased with the sequence:  $\text{PW}_{12}/\text{TiO}_2 \cong \text{SiW}_{12}/\text{TiO}_2 > \text{PMo}_{12}/\text{TiO}_2 > \text{SiW}_{12}/\text{TiO}_2$ -H, which corresponds both to the sequence of the catalytic activity for propene hydration and, at least for the impregnated samples, to that reported in the literature for the bare HPA species [37].

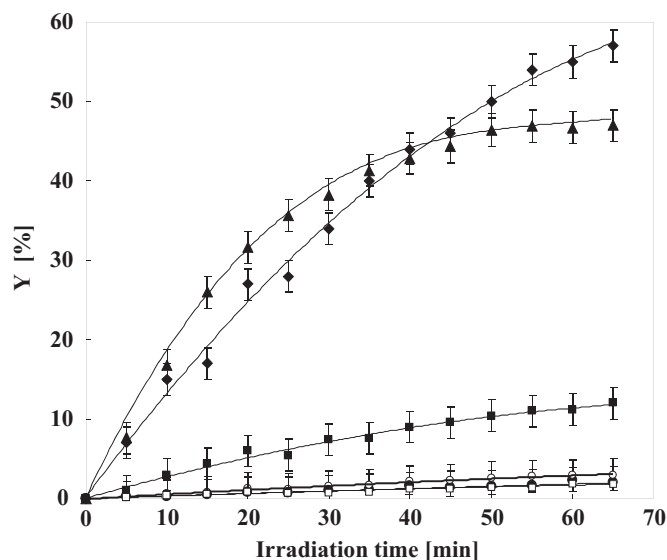


Fig. 8. Acrolein yield (Y%) versus irradiation time for runs carried out in the absence of photocatalyst and in the presence of  $\text{HPA}/\text{TiO}_2$  or bare  $\text{TiO}_2$ . Symbols as in Fig. 7.

## 3.2. Photocatalytic reactivity

### 3.2.1. Photocatalytic propene hydration in gas-solid regime

Fig. 6 shows 2-propanol and di-isopropylether formation rate for catalytic and catalytic photo-assisted hydration of propene and it can be noticed that the presence of light is beneficial for the occurrence of the reaction. Indeed, in any case the catalytic photo-assisted reaction proceeded at higher rate with respect to the catalytic one. Moreover, the  $\text{SiW}_{12}/\text{TiO}_2$ -H sample prepared by the hydrothermal method did not show appreciable activity both in catalytic and catalytic photo-assisted reaction. As far as the formation of 2-propanol is concerned, the catalyst with the best catalytic activity was the  $\text{SiW}_{12}/\text{TiO}_2$  sample, whilst the sample with the best catalytic photo-assisted activity was  $\text{PMo}_{12}/\text{TiO}_2$ . The formation rate of di-isopropylether was, in any case, much lower than the formation of 2-propanol (ca. one order of magnitude) and the catalyst showing the best activity both in the presence and in the absence of light was the  $\text{PMo}_{12}/\text{TiO}_2$  sample.

Preliminary tests carried out under the same experimental conditions, but by using bare  $\text{TiO}_2$  as the catalyst, instead of the binary materials, evidenced that  $\text{TiO}_2$  was inactive for both the catalytic and catalytic photo-assisted propene hydration reaction. This finding evidenced that the active species for the hydration reaction are the heteropolyacid clusters. The catalytic and catalytic photo-assisted activity of an HPA ( $\text{PW}_{12}$ ) supported on  $\text{TiO}_2$ ,  $\text{ZrO}_2$  or  $\text{WO}_3$  has been previously studied and a beneficial role of the light on the reaction rate was observed [6–8]. In this paper it is reported that also other heteropolyacids ( $\text{SiW}_{12}$  and  $\text{PMo}_{12}$ ) supported on  $\text{TiO}_2$ , show a significant increase of the (photo)-catalytic activity with respect to the catalytic one in the hydration reaction. Also in this case the acidity of the HPA is the most important factor for the occurrence of the reaction. Moreover, the increase of the reactivity in the presence of UV light can be explained by considering, as already evidenced, the ability of the semiconductor to transfer electrons from the conduction band to the activated  $\text{HPA}^*$  species [7,38]. Indeed,  $\text{TiO}_2$  directly transfers photo-generated electrons from its conduction band to the interfacial HPA with empty d orbitals to form  $\text{HPA}^-$  species, and consequently the electron-hole recombination is delayed (successively HPA species can be regenerated by following the reaction pathway reported in literature) [8]. Consequently, the different behaviour of the various catalysts (in the presence and in the absence of light) can be justified with the dif-

ferent ability to transfer electrons, mainly depending on the nature of the supported HPA. The most efficient catalyst ( $\text{PMo}_{12}/\text{TiO}_2$ ) reached a quantum efficiency of ca. 2% under the experimental conditions used. The quantum efficiency was determined by considering only the increase of the reacted molecules in the presence of light with respect to the corresponding catalytic run. It is important to underline that the increase of the reactivity obtained by irradiation, in some cases, was very high and in order to obtain the same increase of reactivity by thermal catalysis it would be necessary to raise the reactor temperature of ca. 15–20 °C.

### 3.2.2. Photocatalytic glycerol dehydration in liquid-solid regime

Preliminary runs carried out by using  $\text{HPA}/\text{TiO}_2$  samples in the absence of light indicated that the catalysts were completely inactive. Fig. 7 shows glycerol conversions versus irradiation time for runs carried out both in the absence and in the presence of photocatalyst. The photocatalytic conversion of glycerol increased always by increasing the irradiation time.

The control test carried out in the absence of catalyst but in the presence of UV light evidenced that the photolysis process was slightly effective for glycerol conversion, reaching a value of about 20% after 65 min of irradiation. A quite similar photo-reactivity was also observed in the presence of the two bare  $\text{TiO}_2$  samples although the conversion of glycerol reached about 35% when  $\text{TiO}_2$  P25 was used as the photocatalyst. On the contrary, all of the  $\text{HPA}/\text{TiO}_2$  photocatalysts exhibited higher photocatalytic activity. In particular, it was found that the photocatalytic activity of  $\text{PMo}_{12}/\text{TiO}_2$  was higher than that of  $\text{SiW}_{12}/\text{TiO}_2$  and  $\text{PW}_{12}/\text{TiO}_2$ . In summary, the photocatalytic activities of glycerol dehydration in the liquid phase were in the order  $\text{PMo}_{12}/\text{TiO}_2 > \text{SiW}_{12}/\text{TiO}_2 > \text{PW}_{12}/\text{TiO}_2 > \text{TiO}_2$  P25  $> \text{TiO}_2$ -H. Notably, no tests were carried out in the presence of bare HPA because all of the bare HPA samples used are soluble in water and this work aims to study the photoreactivity only in heterogeneous systems.

Formation of acrolein (its yield is reported in Fig. 8) along with glyceraldehyde and dihydroxyacetone was observed during the photo-conversion of glycerol. For all of the tested catalysts, the acrolein production increased with the irradiation time and it showed to be higher than the value obtained in the experiments carried out in the absence of catalyst or in the presence of bare  $\text{TiO}_2$  samples.  $\text{HPA}/\text{TiO}_2$  photocatalysts were able to promote the dehydration of glycerol and the higher acrolein yield was achieved with  $\text{SiW}_{12}/\text{TiO}_2$  and  $\text{PMo}_{12}/\text{TiO}_2$  samples.

By using  $\text{PMo}_{12}/\text{TiO}_2$ , the acrolein yield was higher than that observed in the presence of  $\text{SiW}_{12}/\text{TiO}_2$ , for an irradiation time lower than 35 min. On the contrary, the reactivity order changed for irradiation times higher than 35 min. This result could be explained by considering that the glycerol conversion on  $\text{PMo}_{12}/\text{TiO}_2$  is almost complete already after 35 min of irradiation and therefore the reaction of acrolein formation slows down.

Fig. 9 shows the glycerol conversion and selectivity to acrolein, respectively, obtained after 65 min of irradiation by using  $\text{HPA}/\text{TiO}_2$ ,  $\text{TiO}_2$  samples and in the absence of photocatalyst. As it can be noticed the selectivity to acrolein was quite different depending on the type of supported HPA, increasing from about 20% for  $\text{PW}_{12}/\text{TiO}_2$  to about 72% for  $\text{SiW}_{12}/\text{TiO}_2$ . On the contrary the selectivity to acrolein obtained with the bare  $\text{TiO}_2$  samples and in homogeneous conditions showed to be similar (ca. 6%) and very low. Therefore, the photocatalyst able to produce acrolein with the highest selectivity was  $\text{SiW}_{12}/\text{TiO}_2$ . Consequently, it was chosen to investigate the influence of the preparation methods on the photocatalytic activity for glycerol dehydration. To this aim a comparison was done with  $\text{SiW}_{12}/\text{TiO}_2$ -H. The results in terms of glycerol conversion and acrolein selectivity versus irradiation time for  $\text{SiW}_{12}/\text{TiO}_2$  and  $\text{SiW}_{12}/\text{TiO}_2$ -H samples are reported in Figs. 10 and 11, respectively.

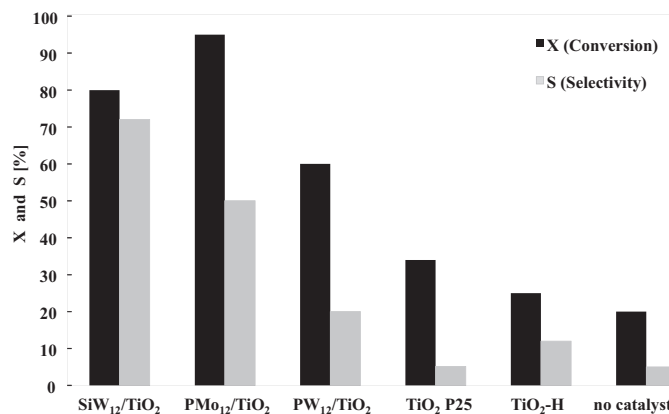


Fig. 9. Glycerol conversion (X%) and acrolein selectivity (S%) after 65 min of irradiation in the presence of  $\text{HPA}/\text{TiO}_2$  photocatalysts, bare  $\text{TiO}_2$  samples and in the absence of photocatalyst.

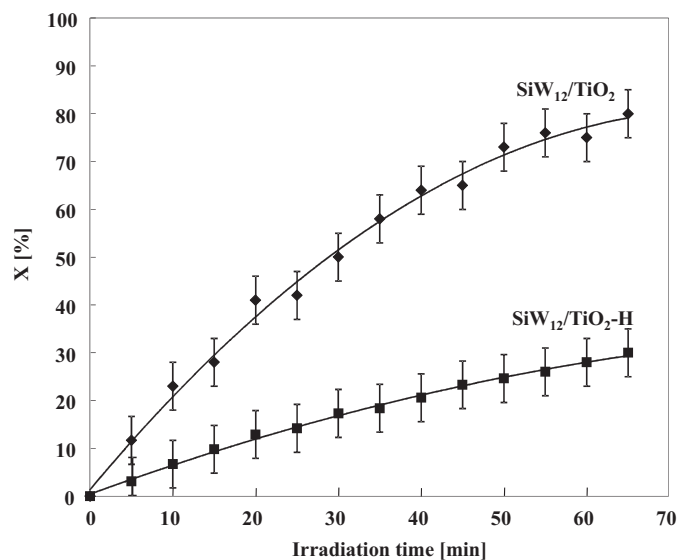


Fig. 10. Glycerol conversion (X%) as a function of irradiation time for runs carried out in the presence of  $\text{SiW}_{12}/\text{TiO}_2$  or  $\text{SiW}_{12}/\text{TiO}_2$ -H photocatalysts.

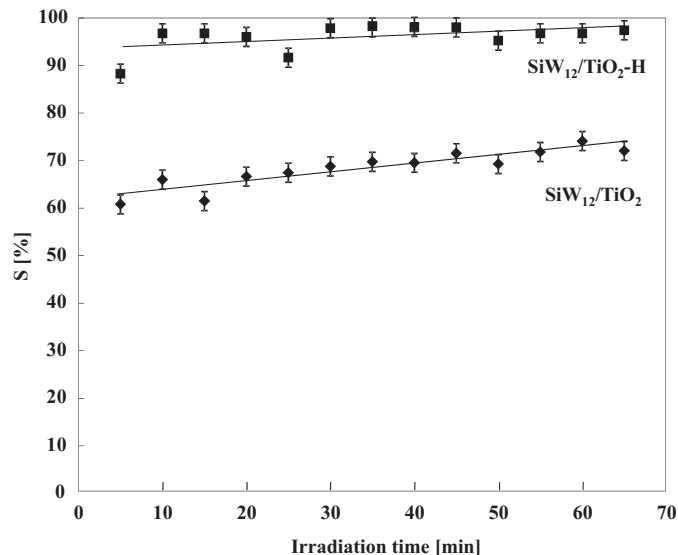


Fig. 11. Acrolein selectivity (S%) as a function of irradiation time for runs carried out in the presence of  $\text{SiW}_{12}/\text{TiO}_2$  or  $\text{SiW}_{12}/\text{TiO}_2$ -H photocatalysts.

For both photocatalysts, glycerol conversion and acrolein yield increased with irradiation time but the photocatalytic performance in terms of glycerol conversion was higher for the SiW<sub>12</sub>/TiO<sub>2</sub> sample. Despite the glycerol conversion in the presence of SiW<sub>12</sub>/TiO<sub>2</sub>-H photocatalyst was lower than that obtained with SiW<sub>12</sub>/TiO<sub>2</sub> (Fig. 10), the acrolein selectivity (Fig. 11) increased from about 70% (SiW<sub>12</sub>/TiO<sub>2</sub>) to 96% (SiW<sub>12</sub>/TiO<sub>2</sub>-H), underlining the importance of the preparation method. The different selectivity was probably due to a lower oxidizing ability of the sample obtained via hydrothermal route (see the photocatalytic results on TiO<sub>2</sub> P25 and TiO<sub>2</sub>-H, Fig. 7). In particular, glycerol conversion in the presence of TiO<sub>2</sub> P25 was higher than that obtained with TiO<sub>2</sub>-H, whereas the acrolein yield was higher by using the latter photocatalyst (Fig. 8). As a consequence the oxidation products (dihydroxyacetone and glyceraldehyde) were obtained in larger amount when TiO<sub>2</sub> P25 was used.

By considering these results the dehydration reaction of glycerol to acrolein was strongly favoured for SiW<sub>12</sub>/TiO<sub>2</sub>-H with respect to SiW<sub>12</sub>/TiO<sub>2</sub>.

As far as the temperature is concerned, the hydration reaction of propene in gas-solid phase and the dehydration reaction of glycerol in liquid-solid phase were differently influenced. In particular in gas-solid phase the hydration of propene started, in appreciable amounts, only at temperatures equal or higher than 85 °C. Moreover the presence of light increased the reaction rate but it is important to underline that the only presence of light was not able to sustain the reaction. On the contrary, the dehydration reaction of glycerol in liquid-phase proceeded at low temperature (35 °C) but only in the presence of light.

As far as the samples reactivity is concerned, the order of reactivity for the propene hydration to 2-propanol in gas phase was: SiW<sub>12</sub>/TiO<sub>2</sub> > PW<sub>12</sub>/TiO<sub>2</sub> > PMo<sub>12</sub>/TiO<sub>2</sub> » SiW<sub>12</sub>/TiO<sub>2</sub>-H under dark conditions and PMo<sub>12</sub>/TiO<sub>2</sub> > SiW<sub>12</sub>/TiO<sub>2</sub> > PW<sub>12</sub>/TiO<sub>2</sub> » SiW<sub>12</sub>/TiO<sub>2</sub>-H in the presence of light. It was the same observed for the glycerol conversion under irradiation in liquid phase, but in this case also the SiW<sub>12</sub>/TiO<sub>2</sub>-H sample showed an appreciable reactivity. The order of reactivity to produce acrolein, instead, was the following: PMo<sub>12</sub>/TiO<sub>2</sub> > SiW<sub>12</sub>/TiO<sub>2</sub> > SiW<sub>12</sub>/TiO<sub>2</sub>-H > PW<sub>12</sub>/TiO<sub>2</sub> after 35 min of irradiation and SiW<sub>12</sub>/TiO<sub>2</sub> > PMo<sub>12</sub>/TiO<sub>2</sub> > SiW<sub>12</sub>/TiO<sub>2</sub>-H > PW<sub>12</sub>/TiO<sub>2</sub> before 35 min of irradiation, although the first two samples showed very similar yield (Fig. 8). Please note that acrolein yield for the run carried out in the presence of SiW<sub>12</sub>/TiO<sub>2</sub>-H was not reported in Fig. 8, but it can be easily calculated by multiplying glycerol conversion by acrolein selectivity (data reported in Figs. 10 and 11). Notably only the hydration reaction of propene to 2-propanol and small amounts of di-isopropylether (without formation of oxidation products) were observed in gas-solid phase. In liquid-solid phase also the formation of oxidation products (glyceraldehyde and dihydroxyacetone), instead, was observed in some cases in addition to the dehydration of glycerol to acrolein. Moreover, not quantified, small amounts of CO<sub>2</sub> and CO were found as volatile species (see Section 2). The exclusive formation of acrolein (with a selectivity close to 100%) was observed only in the presence of SiW<sub>12</sub>/TiO<sub>2</sub>-H. The formation of small amounts of oxidation species was observed also in the runs carried out in homogeneous conditions.

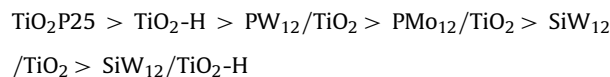
By considering the information deriving from bulk and textural characterization of the photocatalysts it is possible to explain the different reactivity observed for the various samples in the two kinds of systems. As far as the reaction of propene hydration is concerned, the reactivity of the impregnated samples was quite similar under dark condition, but the PMo<sub>12</sub>/TiO<sub>2</sub> catalyst showed the lowest reactivity probably because of the high theoretical coverage onto the TiO<sub>2</sub> surface that this sample presents with respect to the others (4.5 vs. 2.8; see Table 2).

On the contrary, in the presence of light, this photo-catalyst turns the most active, probably due to its lower band-gap with respect to the other samples, and this circumstance allows to exploit more efficiently the light emitted by the lamp. Regarding the SiW<sub>12</sub>/TiO<sub>2</sub>-H sample, it resulted almost inactive for the propene hydration reaction and this finding could be related to the distortion of the SiW<sub>12</sub> cluster in the binary material, evidenced by RAMAN and FT-IR investigations, that inhibits the HPA acid sites responsible for the reaction.

In the case of the reaction system working in liquid-solid phase, the conversion of glycerol, differently from the previous described system, gives rise to the formation of one dehydration compound (acrolein) and also to the formation of two oxidation products (glyceraldehyde and dihydroxyacetone) and it should be considered to better understand the global reactivity of the samples. Consequently, the conversion of glycerol resulted the sum of two different kinds of reactions (dehydration and oxidation) because in the liquid-solid system the presence of water favoured also the oxidation reaction of glycerol, although the reaction was carried out in the absence of molecular oxygen.

It can be concluded that the presence of the heteropolyacid in the binary materials gave rise under irradiation to the dehydration of glycerol while the presence of TiO<sub>2</sub> to oxidation reactions to glyceraldehyde and dihydroxyacetone. Only in the case of the SiW<sub>12</sub>/TiO<sub>2</sub>-H sample the oxidant properties of TiO<sub>2</sub> were almost totally depressed probably because of the lower oxidizing ability for the sample obtained via hydrothermal route.

Moreover, as in the case of propene hydration, the dehydration of glycerol that involves the acid sites of HPA was depressed for the SiW<sub>12</sub>/TiO<sub>2</sub>-H sample, confirming the negative effect of the strong interaction between SiW<sub>12</sub> and TiO<sub>2</sub>. Anyway, it is interesting to note that the selectivity to acrolein observed in the presence of SiW<sub>12</sub>/TiO<sub>2</sub>-H sample was close to 100% because the oxidation reactions were completely inhibited. By comparing the conversion of glycerol and the selectivity to acrolein, it can be hypothesized the following oxidant ability of the tested samples:



Anyway, because the reaction was carried out in the absence of O<sub>2</sub>, the oxidant properties of the powders were, in some cases, depressed and consequently their acid-base characteristics were privileged. The increase in acrolein selectivity is attributed to the presence of HPA on TiO<sub>2</sub> surface in accord with a previous work about the liquid phase catalytic dehydration of glycerol to acrolein [18]. It was suggested that the secondary hydroxyl group of glycerol was firstly protonated, then dehydration occurred to form 3-hydroxypropanal that in turn dehydrated to acrolein [17,39,40]. However, 3-hydroxypropanal was not detected under UV irradiation, indicating that it was rapidly dehydrated to acrolein [18].

#### 4. Conclusions

(Photo)catalytic propene hydration to 2-propanol and photocatalytic glycerol dehydration to acrolein reactions have been successfully carried out by using Keggin heteropolyacids (HPAs) supported on TiO<sub>2</sub>. Binary materials have been prepared by impregnation of H<sub>3</sub>PW<sub>12</sub>O<sub>40</sub>, H<sub>3</sub>PMo<sub>12</sub>O<sub>40</sub> and H<sub>4</sub>SiW<sub>12</sub>O<sub>40</sub>, on TiO<sub>2</sub> Evonik P25. Moreover, a binary material consisting of H<sub>4</sub>SiW<sub>12</sub>O<sub>40</sub> and TiO<sub>2</sub> was prepared via a hydrothermal treatment and tested for the same reactions.

The hydration reaction of propene in gas-solid phase and the dehydration reaction of glycerol in liquid-solid phase were differently influenced by the temperature. In particular in gas-solid phase

the hydration of propene started, in an appreciable amount, only at temperatures equal or higher than 85 °C. Moreover the presence of light increased the reaction rate but the only presence of light was not able to sustain the reaction. On the contrary, the dehydration reaction of glycerol in liquid-phase proceeded at low temperature (35 °C) but only under irradiation. The Keggin HPA species played a key role in (photo)catalytic reactions, due to their strong acidity and their ability to form strong oxidant species gave rise to redox reactions under UV irradiation.

### Acknowledgements

The authors wish to thank MIUR (Rome), Università degli Studi di Palermo and Università degli Studi di Salerno for financial support.

### References

- [1] D. Long, E. Burkholder, L. Cronin, *Chem. Soc. Rev.* 36 (2007) 105–121.
- [2] M.T. Pope, A. Müller, *Angew. Chem Int. Ed. Engl.* 30 (1991) 34–48.
- [3] N. Mizuno, M. Misono, *Chem. Rev.* 98 (1998) 199–217.
- [4] C. Streb, *Dalton Trans.* 41 (2012) 1651–1659.
- [5] A. Hiskia, A. Mylonas, E. Papaconstantinou, *Chem. Soc. Rev.* 30 (2001) 62–69.
- [6] G. Marci, E. García-López, L. Palmisano, *Eur. J. Inorg. Chem.* 1 (2014) 21–35.
- [7] G. Marci, E. García-López, M. Bellardita, F. Parisi, C. Colbeau-Justin, S. Sorgues, L.F. Liotta, L. Palmisano, *Phys. Chem. Chem. Phys.* 15 (2013) 13329–13342.
- [8] G. Marci, E.I. García-López, L. Palmisano, *Appl. Catal. A* 421–422 (2012) 70–78.
- [9] I.V. Kozhevnikov, *Catalysis for Fine Chemical Synthesis. Vol. 2: Catalysis by Polyoxometalates*, John Wiley and Sons Chichester, 2002.
- [10] A. Gervasini, A. Auroux, *J. Catal.* 131 (1991) 190–198.
- [11] Y. Zheng, X. Chen, Y. Shen, *Chem. Rev.* 108 (2008) 5253–5277.
- [12] B. Farin, A.H.A. Monte Verde Videla, S. Specchia, E.M. Gaigneaux, *Catal. Today* 257 (2015) 11–17.
- [13] A. Corma, G.W. Huber, L. Sauvanaud, P. O'Connor, *J. Catal.* 257 (2008) 163–171.
- [14] E. Markočič, B. Kramberger, J.G. van Bennekom, H.J. Heeres, J. Vos, Ž. Knez, *Renew. Sustain. Energy Rev.* 23 (2013) 40–48.
- [15] S.H. Chai, H.P. Wang, Y. Liang, B.Q. Xu, *Green Chem.* 9 (2007) 1130–1136.
- [16] S.H. Chai, H.P. Wang, Y. Liang, B.Q. Xu, *J. Catal.* 250 (2007) 342–349.
- [17] E. Tsukuda, S. Sato, R. Takahashi, T. Sodesawa, *Catal. Commun.* 8 (2007) 1349–1353.
- [18] L. Shen, H. Yin, A. Wang, Y. Feng, Y. Shen, Z. Wu, T. Jiang, *Chem. Eng. J.* 180 (2012) 277–283.
- [19] L. Liu, B. Wang, Y. Du, A. Borgna, *Appl. Catal. A* 489 (2015) 32–41.
- [20] Y. Guo, C. Hu, *J. Mol. Catal. A* 262 (2007) 136–148.
- [21] F. Ma, T. Shi, J. Gao, L. Chen, W. Guo, Y. Guo, S. Wang, *Colloid Surf. A* 401 (2012) 116–125.
- [22] R. Sivakumar, J. Thomas, M. Yoon, *J. Photochem. Photobiol. C* 13 (2012) 277–298.
- [23] O. Sacco, M. Stoller, V. Vaiano, P. Ciambelli, A. Chianese, D. Sannino, *Int. J. Photoenergy* (2012) 8, <http://dx.doi.org/10.1155/2012/626759> (Article ID 626759).
- [24] J. Matos, E. García-López, L. Palmisano, A. García, G. Marci, *Appl. Catal. B* 99 (2010) 170–180.
- [25] A. Micek-Ilnicka, *J. Mol. Catal. A* 308 (2009) 1–14.
- [26] G.A. Trompsett, G.A. Bowmaker, R.P. Cooney, J.B. Metson, K.A. Seatkins, *J. Raman Spectrosc.* 26 (1995) 57–62.
- [27] L. Nakka, J.E. Molinari, I.E. Wachs, *J. Am. Chem. Soc.* 131 (2009) 15544–15554.
- [28] U. Lavrenič Štangar, B. Orel, A. Régis, Ph. Colomban, *J. Sol Gel Sci. Technol.* 8 (1997) 965–971.
- [29] A.K. Cuentas, C. Frausto, L.A. Ortiz-Frade, G. Orozco, *Vib. Spectrosc.* 57 (2011) 49–54.
- [30] A. Popa, V. Sasca, E.E. Kiss, R. Marinkovic-Nedudin, I. Holclajtner-Antunovic, *Mater. Res. Bull.* 46 (2011) 19–25.
- [31] V. Brahmkhatri, A. Patel, *Ind. Eng. Chem. Res.* 50 (2011) 13693–13702.
- [32] R.M. Ladera, M. Ojeda, J.L.G. Fierro, S. Rojas, *Catal. Sci. Technol.* 5 (2015) 484–491.
- [33] M.T. Pope, *Heteropoly and Isopolyoxometalates*, Springer-Verlag, New York, 1983.
- [34] C. Rocchiccioli-Deltcheff, M. Fournier, R. Franck, R. Thouvenot, *Inorg. Chem.* 22 (1983) 207–226.
- [35] A. Bielański, J. Datka, B. Gil, A. Małacka-Lubańska, A. Micek-Ilnicka, *Catal. Lett.* 57 (1999) 61–64.
- [36] J. Tauc, *Mater. Res. Bull.* 3 (1968) 37–46.
- [37] M.N. Timofeeva, *Appl. Catal. A: Chem.* 256 (2003) 19–35.
- [38] T. Tachikawa, M. Fujitsuka, T. Majima, *J. Phys. Chem. C* 111 (2007) 5259–5275.
- [39] W. Suprun, M. Lutecki, T. Haber, H. Papp, *J. Mol. Catal. A: Chem.* 309 (2009) 71–78.
- [40] W. Yan, G.J. Suppes, *Ind. Eng. Chem. Res.* 48 (2009) 3279–3283.